Vol. 64: 39–54, 2015
doi: 10.3354/cr01265

CLIMATE RESEARCH
Clim Res

Published June 17

Contribution to CR Special 30 'Effects of extreme global warming in northern Europe'

Effect of a high-end CO_2-emission scenario on hydrology

Ida B. Karlsson[1,3,*], Torben O. Sonnenborg[1], Lauren P. Seaby[2], Karsten H. Jensen[3], Jens Christian Refsgaard[1]

[1]Geological Survey of Denmark and Greenland (GEUS), Voldgade 10, Copenhagen 1350, Denmark
[2]Department of Environmental, Social, and Spatial Change, Roskilde University, Universitetsvej 1, Building 02, Roskilde 4000, Denmark
[3]Department of Geosciences and Natural Resource Management, Copenhagen University, Rolighedsvej 23, 1958 Frederiksberg C, Copenhagen, Denmark

ABSTRACT: In the latest IPCC report, worst case scenarios of climate change describe average global surface warming of up to 6°C from pre-industrial times by the year 2100. This study highlights the influence of a high-end 6 degree climate change on the hydrology of a catchment in central Denmark. A simulation from the global climate model, EC-Earth, is downscaled using the regional climate model HIRHAM5. A simple bias correction is applied for daily reference evapotranspiration and temperature, while distribution-based scaling is used for daily precipitation data. Both the 6 degree emission scenario and the less extreme RCP4.5 emission scenario are evaluated for the future period 2071–2099. The downscaled climate variables are applied to a fully distributed, physically based, coupled surface–subsurface hydrological model based on the MIKE SHE model code. The impacts on soil moisture dynamics and evapotranspiration show increasing drying-out tendencies for the future, most pronounced in the 6 degree scenario. Stream discharge and groundwater levels also show increased drying due to higher evapotranspiration. By comparing the 6 degree scenario with other emission scenarios, it is found that the most prominent changes in the water balance are caused by drying out of soils rather than precipitation effects.

KEY WORDS: Climate change · High-end scenarios · Hydrological modelling · Impact study

1. INTRODUCTION

During the last decade the number of hydrological impact studies has been increasing, and several studies have been published trying to quantify future hydrological changes using climate model outputs on both global (e.g. Arnell 1999), national (e.g. Bergstrom et al. 2001), and regional (e.g. van Roosmalen et al. 2007) scales. The need for ensemble approaches in climate change impact studies has been highlighted several times (e.g. Déqué et al. 2007) to encompass more of the uncertainties arising from emission scenarios as well as climate models and downscaling techniques. Impact studies have therefore increasingly focused on different combinations of scenarios, models, and techniques. Emission scenarios have traditionally been based on projections defined in Nakicenovic et al. (2000) and later by van Vuuren et al. (2011).

The most recent IPCC report (Collins et al. 2013) describes the possibility for high-end scenarios like RCP8.5 with a global climate warming of over 4°C at the end of the 21st century. Changes in this range will have profound effects on hydrology and vegetation, with a potential for increasing in large ecological and economic impacts such as water shortage, wildlife loss, crop failure, flooding, and droughts. The hydrology of a high-end scenario has however not yet been documented.

*Corresponding author: ika@geus.dk

Publisher: Inter-Research · www.int-res.com

The objective of this study is to assess the hydrological impacts for a high-end emission scenario (with a 6°C warming), from here onwards referred to as the 6 degree scenario, compared to impacts for a medium emission scenario. Due to the unusually warm climate projection used in this study, it is logical to focus primarily on consequences of drying effects within the hydrological system. Since the study area is primarily an agricultural area, we decided to emphasise factors affecting crops. This is done using the agricultural drought indices soil moisture deficit index (SMDI) and evapotranspiration deficit index (ETDI) (Narasimhan & Srinivasan 2005).

2. STUDY AREA

The study area is a sub-catchment in the Odense Fjord Basin, located on the island of Funen in central Denmark (Fig. 1). The Odense River drains the 1025 km^2 basin running from mid-Funen into the Odense Fjord in the northeast. In this study, the focus is on the upstream 486 km^2 large sub-catchment with an average river discharge of 4.6 m^3 s^{-1} (1991–2010). The topography in the area varies from ~12 to 129 m from the river valley to the moraine hills. Climatologically, the area is temperate and wet with an annual mean temperature of 8.8°C and precipitation of 808 mm yr^{-1} (1991–2010). The Odense Fjord Basin is comprised of mostly agricultural lands (68%) with some urban areas (16%), woodlands (10%) and a smaller percentage of natural areas (6%) like wetlands, lakes, meadows, and grasslands. The predominant crops are spring and winter cereals, constituting 23 and 45%, respectively, of all farmland (Environment Centre Odense 2007). The geology in the catchment is dominated by end moraines to the south and southwest, and moraine hills to the southeast and northwest. Clayey moraine deposits dominate the area itself; however, aquifers constituted by meltwater sand and gravel deposits are also present (Troldborg et al. 2010).

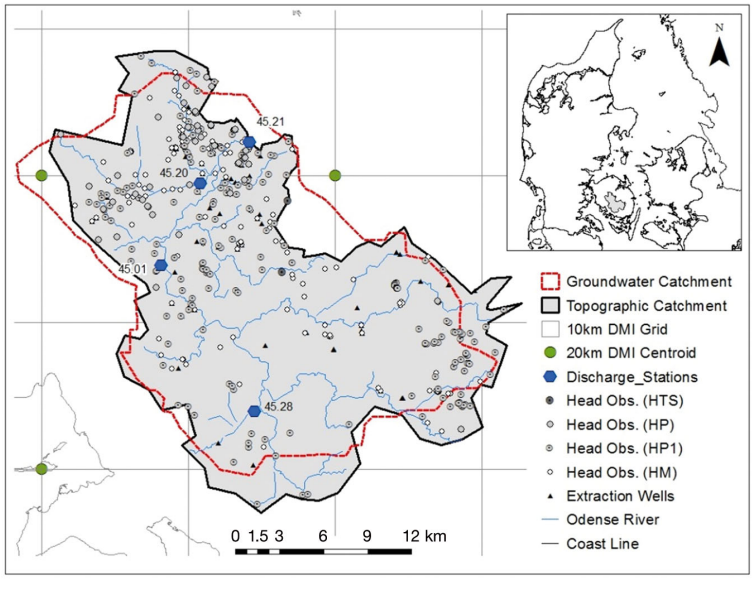

Fig. 1. Study area: Odense Fjord Basin, Denmark

3. METHODS

3.1. Hydrological modeling code

MIKE SHE originates from the Systeme Hydrologique Europeen (SHE) modelling system (Abbott et al. 1986) and is now a coherent modelling framework by DHI Water and Environment. The model is fully distributed and physically-based, and includes descriptions of the following processes: evapotranspiration, snow melt, overland flow, channel flow, unsaturated zone flow, drainage pipe flow, and groundwater flow. For each of these processes different numeric engines are available. The processes are calculated separately but are coupled 2-ways in every time step. All spatially distributed input data are pre-processed into grid based files of the specified grid size. Channel flow is handled by the MIKE-11 model using a kinematic routing description. The saturated flow is calculated using a 3D finite difference scheme, which is a fully distributed and physically based solver (DHI 2009b).

3.2. Emission scenarios and climate models

The basis of this study is the 6 degree high-end emission scenario; it is an idealized scenario, meaning that the run is not based on projected emissions but rather a forced CO_2-development. The atmospheric CO_2 concentration is specified to increase from a pre-industrial level with a rate of 1% yr^{-1} and serves as input to the global coupled atmosphere–ocean–sea ice model EC-Earth (Hazeleger et al. 2012). The model reaches a 6 degree warming at an atmospheric CO_2-concentration of ~1423 ppm. Hereafter, the model is run with a fixed CO_2 concentration for 29 yr. In this period the global mean surface temperature continues

to slowly increase and stabilize at a level of about 6.5 K above pre-industrial level. These 29 yr are then used to represent the years 2071–2099 as a 6 degree warming. Dynamic downscaling is carried out using the RCM HIRHAM5 (Christensen et al. 2007), see Christensen et al. (2015, this Special) for a detailed description. Results from the same general circulation model/regional climate model (GCM/RCM) pairing forced by historical data from the period 1961–2005 were used to establish the bias correction for the control period (see below).

The RCP4.5 emission scenario was also run through the same climate and hydrological model framework to provide data for comparison. The RCP4.5 scenario is based on a real emission projection founded on work by Smith & Wigley (2006), Clarke et al. (2007) and Wise et al. (2009). The RCP4.5 owes its name to the maximum radiative forcing of 4.5 W m^{-2} reached at the end of the century, followed by a stabilization of constant forcing thereafter (Thomson et al. 2011). This forcing is equivalent to a CO_2-concentration of ~540 ppm (Meinshausen et al. 2011) and results in roughly 2 degrees warming at the end of the century. Additionally, results from the study by Karlsson et al. (2014) for the same area using alternative climate models from the ENSEMBLES project (Hewitt & Griggs 2004) and the A1B emission scenario (Nakicenovic et al. 2000) are also included as an additional impact reference. The A1B scenario corresponds approximately to a radiative forcing of 6 W m^{-2} and 700 ppm CO_2-concentration at the end of the century (IPCC 2001).

Whereas results on temperature and precipitation are used directly from the RCM, daily reference evapotranspiration is estimated using the FAO Penman–Monteith equation (Allen et al. 1998) based on RCM output such as incoming and outgoing, short- and long-wave radiation, temperature, water vapor pressure, and wind speed.

3.3. Bias correction

The choice of bias correction method is based on a study by Seaby et al. (2013). They used different GCM/RCM couplings from the ENSEMBLES project (Hewitt & Griggs 2004) investigating the different responses of climate change for 6 Danish regions on a 10 km grid. Two different downscaling methods were evaluated: the delta change approach (DC) and a distribution-based scaling method (DBS; Piani et al. 2010). The DC approach was used on observed data of temperature, precipitation and reference evapotranspiration (potential evapotranspiration for a well-watered grass of uniform height) while applying a monthly change factor (RCM control to future, indirect use of climate data). The DBS method was applied for precipitation using double gamma distributions combined with a dry day correction on a seasonal basis. This method was used along with a bias removal (BR) method on reference evapotranspiration and temperature that also uses the simulated future RCM data directly. Here, the difference (bias) between the observation data and the RCM control period data is perturbed onto the simulated future data. Seaby et al. (2013) showed that the DBS and the DC approach were equally good at reproducing changes in the mean, but the DBS was superior in preserving the variance as well as capturing the precipitation extremes. In a subsequent analysis Seaby et al. (2015) found that a DBS downscaling for each individual grid resulted in reduction of spatial biases between RCM control data and observed data.

The climate model inputs in this study are thus downscaled using DBS for precipitation and BR for reference evapotranspiration and temperature. The historical control period is 1991–2005, while the future period covers 2071–2099. Both the BR and DBS methods are applied on a grid-by-grid basis for each season.

3.4. CO_2-crop factor

Increases in CO_2-concentrations have been shown to affect the stomatal conductance of the leaf surface for plants (Kimball et al. 1993), meaning that higher levels of CO_2 allow the plant to reduce the stomata opening, thus lowering water vapor loss resulting in reduced evapotranspiration (Samarakoon & Gifford 1995, Kimball et al. 1999, Conley et al. 2001, Krujit et al. 2008). This response is somewhat uncertain as other influences are still debated. In this study the approach by Rasmussen et al. (2012) is adopted, where CO_2 sensitivities of leaf conductance, relative transpiration, and transpiration share of the evapotranspiration are multiplied by the relative CO_2 increase. Wheat was chosen as a representative crop, as cereals are by far the most common in the catchment. Using the empirical and experimental values from Rasmussen et al. (2012), a plant correction was multiplied onto the 2 emission scenarios' annual CO_2 change (Meinshausen et al. 2011) and subsequently perturbed onto the RCM reference evapotranspiration. Hydrological model runs were done both with and without this correction.

3.5. Agricultural drought index

To describe agricultural drought, the Soil Moisture Deficit Index (SMDI) and Evapotranspiration Deficit Index (ETDI) were developed by Narasimhan & Srinivasan (2005); They applied the indices for each sub-basin on simulated data from the SWAT model (Arnold et al. 1998) for 6 catchments in Texas, USA. The results showed that both indices are well correlated with actual crop yields on the sites.

The SMDI uses the soil moisture deficit, which is based on weekly soil moisture data from the model and median soil moisture as well as minimum or maximum soil moisture in a reference period. The SMDI is a result of the soil moisture deficit and the SMDI of the previous week. Similarly, the ETDI is based on the weekly water stress anomaly, where the anomaly includes the median and minimum or maximum water stress ratio in a reference period. This ratio is calculated as the difference between potential and actual evapotranspiration, divided by the potential. The ETDI is a product of the water stress anomaly and the ETDI of the previous week. Both indices range between −4 and +4.

In this study, the indices ETDI and SMDI for the top 30 cm soil column are applied in a similar fashion as in Narasimhan & Srinivasan (2005); however, here the indices are applied at the grid scale and used to assess future data as well as historical data. To remove potential climate model biases, the indices are based on GCM/RCM data for both periods. The median, maximum, and minimum water contents (SMDI) and water stresses (ETDI) are based on data from the reference period (1991–2005). Hence, the same values of, for example minimum water content, are used to calculate the indices for the historical and future periods, and this means that the index range may go outside the normal ±4, as lower minimum and higher maximum values may be found in the future climate data. The choice to preserve the historical statistics as basis was chosen in order to compare future results with a known period of reference. If the complete dataset (historical and future) was chosen as basis for the statistics, the SMDI and ETDI in the historical period could not have been assumed to be correlated to the actual yield.

4. MODEL SETUP

MIKE SHE has been used extensively in the Danish National Water Resources model (DK-model) (Henriksen et al. 2003), developed at the Geological Survey of Denmark and Greenland (GEUS). The DK-model comprises 7 model domains covering the whole of Denmark (Højberg et al. 2013). The model domain covering Funen (Troldborg et al. 2010) has been used as point of departure for setting up the MIKE SHE model used in this study.

4.1. Boundary conditions and numerical setup

The groundwater catchment falls outside the topographical catchment by 12%, while 14% of the topographical catchment is outside the groundwater catchment (Fig. 1). Flow in the area is dominated by near-surface processes including overland flow, drain flow, and shallow groundwater flow. Hence, to minimize potential water balance errors the topographical catchment is used to delineate the model boundary. As horizontal boundary conditions in the model, zero flux is applied on all borders as it is assumed that the catchment boundaries represent hydrological divides. The horizontal discretisation of the model is 200 × 200 m, resulting in a total of 12 630 grids covering the whole catchment. The unsaturated flow is determined by the full Richards equation and discretized using a cell spacing of 5 cm in the top 30 cm of the soil column, with cell sizes increasing to 1 m cells at depths below 10 m. The number of layers therefore depends on the depth of the groundwater table (e.g. 12 layers if the groundwater table is at 1 m depth). The saturated zone is resolved by 7 computational layers, and the flow is calculated using a 3D finite difference scheme (DHI 2009b). Maximum time step is specified to 12 h for the overland flow and unsaturated zone, and 24 h for the saturated zone.

In connection with the farming and households within the catchment, there are 103 extraction wells. There is no irrigation in the catchment. Based on the Danish National Well database, Jupiter (GEUS 2014), reported extraction rates are used for the historical simulation period while fixed rates are used from 2012 onward.

4.2. Soil type

The soil data is based on 13 different soil types (Greve et al. 2007) distributed in 3 soil horizons: A, B, and C. This gives rise to potentially almost 2200 soil column combinations. Due to computational limitations, 50 type-soil profiles were generated based on the most common A-, B-, and C-horizon combina-

tions (Børgesen et al. 2013). In this study, the 10 occuring type-soil profiles in the catchment with different A-, B-, C-horizon soil properties are listed here with area coverage (%) and soil profile number (in parentheses): 0.1% moraine sand soil (16); 1% diluvial sand soil (18); 15% moraine clay soil (37); 15% diluvial sand soil (38); 0.4% moraine sand soil (46); 12% moraine clay soil (47); 10% diluvial sand soil (48); 33% moraine clay soil (67); 11% diluvial sand soil (77); and 4% freshwater sand soil (998).

4.3. Land use

Land use in the area is divided into 12 categories; 3 covering natural landscapes: grassland (5%), deciduous forest (3%), and coniferous forest (2%); 7 covering farm lands: 3 types of dairy farms (18%), 2 types of pig farms (48%), and 2 types of plant production (16%); one category covering hydrology in the form of water bodies (1%); and one category covering urban areas (8%).

In reality, farm type dependent crop rotation schemes are used at each individual field. To simplify the description, the farm type's crop rotation is translated into a relative distribution of crop types within each of the 7 farm types (Table 1), which results in 12 different crop types recognized in the catchment; however, only 8 different crop inputs are used, as some crop types are very similar and are thus treated as one (Table 1). For each of the 8 crop types, information about the crop parameters including leaf area index and root depth are available from DAISY model runs for the period 1990–2010 (Børgesen pers. comm.). DAISY (Hansen et al. 1990) is a root zone model that is physically based and simulates nitrate and carbon transport/transformation and water flow based on agricultural practices.

As the crop parameters not only depend on crop type but also on soil type, the crops are distributed such that the relative distribution is preserved within each land use–soil combination. Spatially, the grids are distributed randomly on the grid map in the cells with the appropriate land use–soil combination. The 5 additional land use categories are represented by one 'crop type' only: the forests by deciduous and coniferous trees, urban areas and water bodies by 'crops' specified to these categories, and the grassland is represented by the farm land crop type of grass. Finally, this results in a grid map where the 12 crop types and 10 soil types in combination yield 107 different crop–soil matches in total for the whole catchment.

4.4. Geology

The geology in the area is divided into units with similar hydraulic properties and is based on the work done in connection with the DK-model (Troldborg et al. 2010). The area contains 11 geological units, constituting 4 hydro-stratigraphic layers. The first layer contains the top 3 m with the geological units of top sand, top clay, top chalk, top moraine clay, peat, and other distributed on the basis of a geological map. The first layer covers the unsaturated zone and the top of the saturated zone. The second layer is a fractured

Table 1. Relative crop distribution within each farm type

Crop	Farm types							% of agricultural cells
	Plant/mixed	Pig/plant	Pig	Dairy 1	Dairy 2	Dairy 3	Unknown/mixed	
Maize	0.2	5.3	0.7	2.6	18.3	31.3	1.4	5
Grass								21
Grass	1.8	4.7	0.6	5.5	15.7	15.7	6.4	
Pasture	3.6	4.1	2.1	14.3	7.8	5.3	28.2	
Grass Seeds	9.1	5.7	5.6	6.8	2.5	0.7	5.1	
Barley								20
Spring Cereal	22.9	23.8	21	27.2	19.2	16	14.5	
Legume	0.6	1.2	0.3	0.2	1	0	0.2	
Winter Wheat	38.1	35.9	50	26.8	20.3	18.9	19.7	35
Winter Rape	4	4	7.6	2.3	2.6	3.7	1.8	5
Potatoes	1.3	1.2	0.3	0.2	0.6	0	0.5	1
Sugar beets								5
Vegetable	1	1.4	0.4	0.8	0.3	0	2.9	
Sugar Beets	5.5	4.5	4.8	4.5	3.3	3.5	2.2	
Fallow	11.9	8.1	6.7	8.7	8.4	4.9	17.3	8
% of agricultural cells	12	22	36	3	14	5	7	–

clay layer. The third layer is a low permeable formation consisting of moraine clay, post-glacial clays, and silts (geological units: quaternary clay). Below the third layer, pre-quaternary deposits containing low permeable clays and chalk from Danien (geological units: pre-quaternary clay, pre-quaternary fractured clay, pre-quaternary chalk) are situated. Within these 4 layers, 3 sand bodies consisting of outwash sands and gravel (geological units: outwash sand) are recognized and constitute the aquifers in the area. The middle sand lens represents the aquifer with the largest extent and thickness (Nyegaard et al. 2010).

4.5. Time varying input data

Daily values of precipitation, temperature, and reference evapotranspiration are specified as input to the model. As precipitation input, the 10 km DMI grid data (Scharling 1999) (Fig. 1) with dynamic gauge catch correction (Stisen et al. 2012) are used. Data for temperature and reference evapotranspiration, calculated by Makkink's formula (Makkink 1957), are specified as 20 km grid values (Fig. 1).

5. CALIBRATION

The model is run for the period 1990–2010, where 1990–1999 is used as a spin-up period, and is calibrated for the period 2004–2007. There are 2 validation periods, one before (2000–2003) and one after (2008–2010) the calibration period. The AutoCal scheme incorporated in the MIKE SHE software is used as the autocalibration tool (DHI 2009a). The most sensitive parameters were identified by a sensitivity analysis prior to the calibration.

5.1. Calibration data

The catchment includes 4 discharge stations with data in the calibration period: Stns 45.21, 45.01, 45.28, and 45.20 (see Fig.1). There are 455 wells with hydraulic head observations in the catchment. The wells are divided into 4 categories: H_{TS}, H_P, H_{P1}, and H_M. H_{TS} contains 5 wells with long time series (>3000 observations) within the calibration period. H_P contains 63 wells that only have a few observations within the calibration period. H_{P1} contains 209 wells with only 1 observation within the calibration period. The last category, H_M, holds the remaining 178 wells; these wells have no observations within the calibration period; however, their measurements are used as average values for hydraulic head (calculated outside the calibration period).

5.2. Objective function

The objective functions are based on the performance criteria water balance (WB) and RMSE:

$$f(\theta)_{\mathrm{WB},X} = \sum_{k=1}^{K}\left(\frac{1}{n}\sum_{i=1}^{n}(O_i - S_i)\right) \quad (1)$$

$$f(\theta)_{\mathrm{RMSE},X} = \sum_{k=1}^{K}\left(\frac{1}{n}\sum_{i=1}^{n}(O_i - S_i)^2\right)^{1/2} \quad (2)$$

where n is the number of time steps, O_i and S_i are observed and simulated values at time $i = 1, 2, \ldots, n$, for $k = 1, 2, \ldots K$, where K is number of stations or wells. A subscript, X, after the objective function type (WB or RMSE) indicates whether the objective function is based on discharge values (Q) or on head measurements (H_{TS}, H_P, H_{P1} or H_M). For the calibration scheme, a total of 6 different objective functions are used.

The objective functions for the 4 discharge stations are aggregated such that the total objective function value is simply a summation of all stations, ensuring that small sub-catchment stations have smaller contributions to the overall objective function. Station 45.28 is situated just downstream lake Arreskov Soe, and the outflow from the lake is highly influenced by human regulations, which makes it difficult to reproduce the temporal variability of the outflow from the lake. Therefore, the station is only included in the objective function for WB. The multiple objection function, within the predefined parameter space (θ) is defined as:

$$F(\theta) = \min\{f(\theta)_{\mathrm{WB},Q}; f(\theta)_{\mathrm{RSME},Q}; f(\theta)_{\mathrm{RSME},H_{TS}}; f(\theta)_{\mathrm{RSME},H_p}; f(\theta)_{\mathrm{RSME},H_{ps1}}; f(\theta)_{\mathrm{RSME},H_M}\} \quad (3)$$

5.3. Optimization algorithm

The Population Simplex Evolution method (PSE; DHI 2009a) is used as the optimization algorithm in this study.

The stopping criterion is defined by either the maximum number of model evaluations or a convergence in the objective function space. This means that the objective function of the best parameter set has not changed more than a given value within a number of shuffling loops or a convergence in the parameter space, so the range of parameter values of the entire population is less than a given value (DHI 2009a).

6. RESULTS

6.1. Parameter sensitivity and parameterization

The MIKE SHE model has an extensive and complex setup and as such contains many parameters available for calibration. To decrease calibration time and to avoid non-uniqueness problems, the number of parameters has to be limited to the most sensitive set. To determine the most sensitive parameters for this model setup, 28 parameters were tested in a sensitivity analysis using the scaling procedure described by Hill (1998). The parameters investigated in the river and drainage system are the drain depth, the drainage time constant, and the stream leakage coefficient. For the unsaturated zone, the saturated hydraulic conductivity, as well as the van Genuchten parameters *n* and alpha for 2 soils (37 and 38) were chosen. Soil 37 is a clay type soil and tied to this value are the other dominating clay soils: 47, 67, and 68. Soil 38 is a sandy soil, and the other sandy soil, no. 48, is tied to this value. The values are tied individually for all 3 soil horizons: A, B and C. In the saturated zone the horizontal hydraulic conductivity for the geological units top sand, top moraine clay, outwash sand, quaternary clay, pre-quaternary clay with and without fractures and pre-quaternary chalk are investigated. The vertical hydraulic conductivities are tied to the horizontal values using an anisotropy factor of 10 for all but the top moraine clay where a factor of 100 is used.

This results in a total of 71 parameters where only 28 are free. The result of the aggregated sensitivity analysis is shown in Fig. 2A. The 10% limit denotes 10% of the sensitivity of the parameter with the highest sensitivity value here given by the horizontal conductivity for the quaternary clay. However, a further investigation of the parameter sensitivity for the individual objective functions shows that for the 2 least sensitive parameters above the 10% limit, the saturated hydraulic conductivity for soil 37 in horizon B is only sensitive for 1 objective function type, while the *n* parameter for soil 37 in horizon C is only sensitive for 2 objective function types (not shown). It was therefore chosen only to select the horizontal hydraulic conductivity for the outwash sand, the quaternary clay, and the chalk; as well as the time constant for the drains and the saturated conductivity for soil 37 of horizon C for calibration. Initial parameter values were based on the optimal parameter values from the DK-model.

6.2. Calibration and validation results

The calibration required 285 simulations to reach a satisfactory solution for the 5 parameter values (Fig. 2B). The resulting hydrograph for the main station can be seen in Fig. 2C. A relatively low WB error of −3% is found, indicating a small tendency for the model to overestimate the discharge. The Nash-Sutcliffe coefficient indicates a high degree of covariance between observed and simulated data. The plots in Fig. 2D,E show the WB and Nash-Sutcliffe coefficients for the 4 stations for both validation and calibration periods. Still looking only at the main station (Stn 45.21), the WB error is slightly elevated in the validation periods 2000–2003 and 2008–2010, while the Nash-Sutcliffe coefficient is very similar to the calibration period.

The signal is similar for Stn 45.20 as for the main station, but the performance is poorer. The poorer performance may partly be due to the smaller size of the catchment and may be affected by the non-accounted differences between the groundwater and the topographical divides in this area. It should be noted that observed data only exists for 2000–2003 and 2005. Therefore, no data are available for the second validation period. The performance for Stn 45.28 is generally low; however, this is not surprising as the hydrograph for this station is highly affected by human regulation at the outlet from the lake. Stn 45.01 has a high Nash-Sutcliffe coefficient for both validation and calibration periods. Both water balance and RMSE show elevated values in the calibration period compared to the validation periods. The reason for these discrepancies seems to originate partly from 2 peaks in the observed data in June/July and December 2007, as the WB error is reduced to 8.5% and the RMSE to 1.17 mm without these months.

The plot in Fig. 2F shows the RMSE for the 2 head objective functions H_{TS} and H_M. The H_P is not shown as few wells have measurements in the whole period, and H_{P1}-wells only have measurements in the calibration period. The H_M shows that the model performs almost equally well on the mean hydraulic head in the validation periods as in the calibration period. The H_{TS} cannot be directly compared across the 3 periods as there are a different number of measurements which the RMSE is based on, for instance, only 3 of the H_{TS}-wells have any data in the last validation period.

6.3. Downscaled climate results

The results of the downscaled climate data are presented in Fig. 3 using change factors. The 6

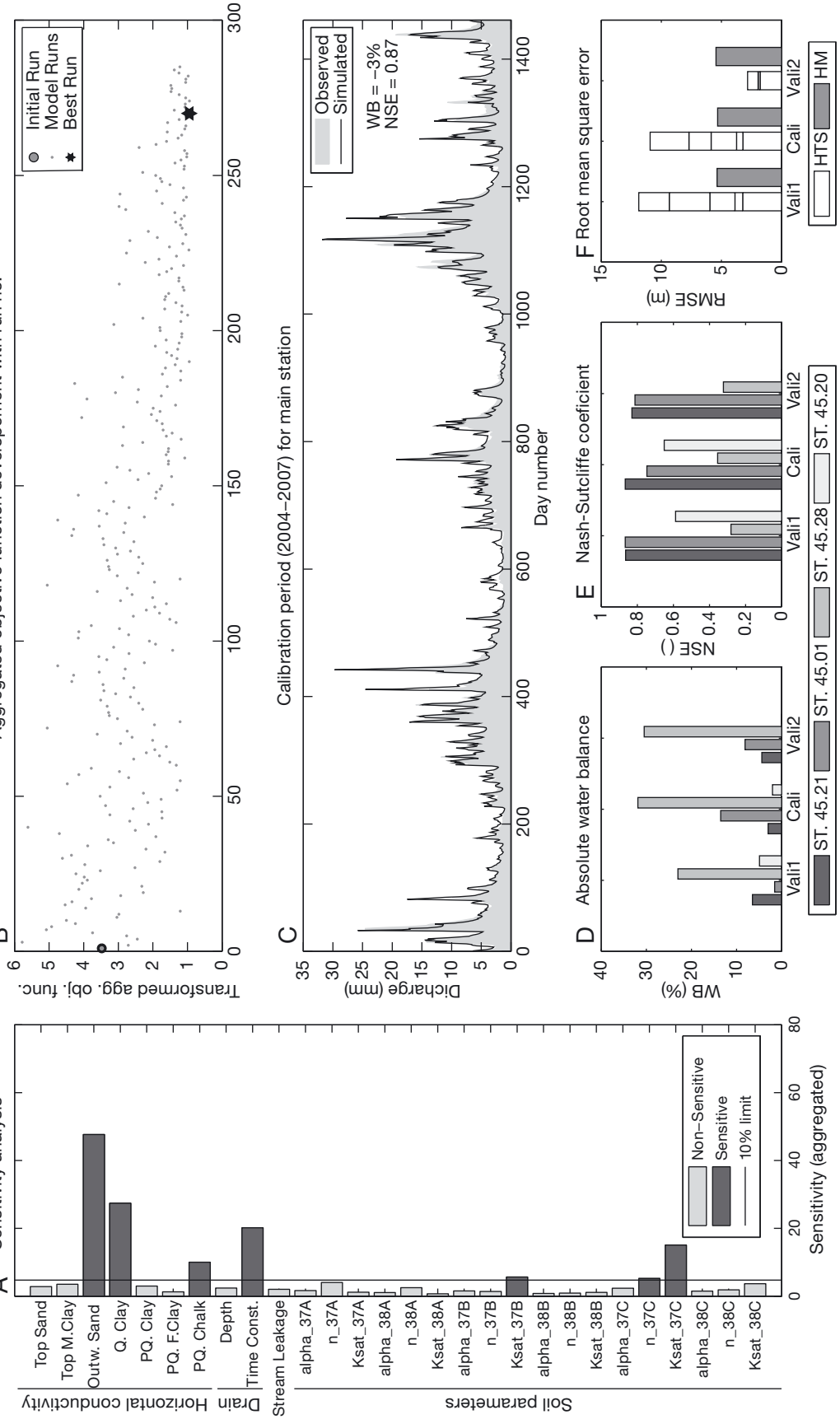

Fig. 2. (A) Sensitivity analysis of the chosen 29 parameters in the MIKE SHE model. 10% limit: 10% of the parameter with the highest sensitivity; Sensitivity: aggregated sensitivity across all 6 objective functions. (B) Change in the transformed and aggregated multiple objective function with model run number during the calibration. *Best run: final model run chosen. (C) Hydrograph for the final model run for the main discharge station (Stn 45.21) in the catchment; with water balance (WB) and Nash-Sutcliffe coefficient for streamflow (NSE). (D,E) WB values and Nash-Sutcliffe coefficients for each of the 4 discharge stations, and (F) RMSE for 2 of the heads objective functions (H_{TS} and H_M) in the calibration (cali; 2004–2007) and validation periods 1 and 2 (vali; 2000–2003 and 2008–2010)

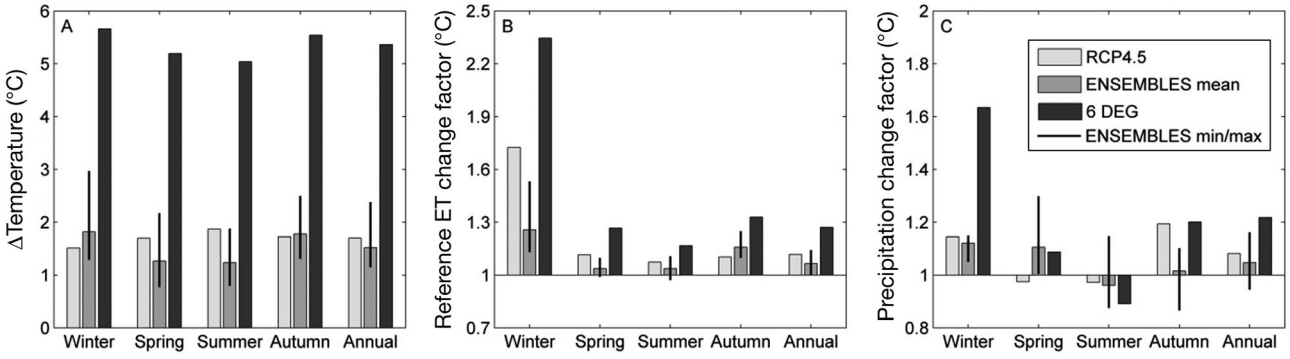

Fig. 3. Bias corrected climate variables for Funen for the 2 emission scenarios: RCP4.5 and 6 degree. Mean of the 4 ENSEMBLES models: ECHAM5-HIRHAM5, ECHAM5-RCA3, ARPEGE-RM5.1 and HadCM3-HadRM3, and an indication of the minimum and maximum values of the 4 simulations (vertical line). (A) Relative change of mean temperature. (B) Change in reference evapotranspiration (ET) without CO_2-correction. (C) Change factors for the mean precipitation

degree emission scenario results in an annual change in temperature of 5.4°C (Fig. 3A), while the RCP4.5 induce an increase of 1.7°C. The distribution of the change is somewhat evenly spread across the seasons. For both emission scenarios the reference evapotranspiration increases (Fig. 3B), with the winter season experiencing the largest relative increase (this reference evapotranspiration is downscaled data without CO_2-correction applied). For precipitation (Fig. 3C), the signal of the 2 scenarios are quite different. Both agree on an annual increase in precipitation. For the RCP4.5, winter and autumn show an increase in precipitation, with autumn being the largest, while summer and spring precipitation are decreasing. For the 6 degree scenario, however, the largest increase is found by far for the winter precipitation, with spring and autumn having smaller increases, while only summer shows a decrease in precipitation.

Fig. 3 also shows the mean change values for 4 ENSEMBLES models from the study by Karlsson et al. (2014). The 4 models ECHA M5-HIRHAM5, ECHAM5-RCA3, ARPEGE-RM5.1, and HadCM3-HadRM3 represent a dry, wet, warm, and medium scenario for Denmark, respectively. The vertical line on the plot indicates the maximum and minimum value for the models. For some seasons and variables, the difference between the 4 models is smaller than the difference between the signals from the emission scenarios (A1B and RCP4.5 compared to the 6 degree). It is seen that the results from the RCP4.5 scenario are close to the mean of the ENSEMBLES results with respect to reference evapotranspiration and precipitation, and to some degree temperature.

6.4. Use of CO_2-crop factor

The CO_2-correction resulted in a 4% reduction of reference evapotranspiration for the RCP4.5 emission scenario compared to the non-corrected RCP4.5 reference evapotranspiration, while the 6 degree scenario resulted in a 24% reduction. For comparison, the A1B emission scenario results in a reduction of 7% using the same procedure (Karlsson et al. 2014). The effect on the reference evapotranspiration compared to the baseline period can be seen in Table 2, along with other major hydrological variables. As the evapotranspiration is lower when the CO_2-correction is used, it is not surprising that the model response is overall wetter; however, for the 6 degree scenario the CO_2-correction actually leads to a complete signal reversal of the changes in actual evapotranspiration, stream discharge and groundwater level. The reduction in evapotranspiration from the 6 degree scenario seems extreme, and it raises the question of whether this correction factor type is valid when dealing with high-end scenarios with large CO_2-changes. Especially considering the still debated extent of the CO_2-effect and possible feedback, it was therefore chosen to continue further analysis of the simulation results without including the CO_2-correction on the reference evapotranspiration.

6.5. Discharge and groundwater

The mean monthly discharge of the main station can be seen on Fig. 4A. The station has high discharge in the winter and low discharge during

Table 2. Change in annual mean flux (mm) from RCM historical control period (1991–2005) to future period (2071–2099) (mm). 6 DEG: high-end 6 degree emission scenario

	Precipitation	Actual evapotranspiration	Discharge main station	Mean hydraulic head (Layer 6)
Without CO_2-correction				
RCP45	+50	+37	+25	+100
6 DEG	+58	+86	−19	−96
With CO_2-correction				
RCP45	+50	+22	+39	+171
6 DEG	+58	−12	+77	+348

summer. When imposing the climatic changes defined by the 2 climate scenarios, the result is an overall increase in discharge for the RCP4.5 and a decrease for the 6 degree scenario (Table 2). Fig. 4B shows that the increase in discharge for the RCP4.5 is primarily a result of large increases in discharge for December to March, while the response is fairly close to control period values for the other months. The 6 degree scenario results in large increases in discharge during January and February as well as noteworthy reductions in April to November. The signal from the station further upstream (Stn 45.01) is similar to the main station (not shown), while the tributary station (45.20) shows decreasing discharge for both scenarios for all months except July in the RCP4.5. The smallest station (45.28) shows decreasing discharge all year with the exception of December for the 6 degree scenario. Decreasing discharge is found in January to September (July increase excluded), and increasing discharge in October to December for the RCP4.5.

The change in hydraulic head can be evaluated in Fig. 5. The hydraulic head in the catchment is generally highest in the northwest, southwest and southeast corners of the catchment; while the lowest hydraulic head is found in the downstream end of the river valley. For the RCP4.5 scenario there is a mean groundwater level rise of 0.8 to 1.4 m in the southwestern part of the catchment, while the rest of the catchment is relatively unchanged. However, for the maximum values it is apparent that the scenario also results in a reduction in the maximum heads in the north and an increase in maximum level in south. For the 6 degree scenario there is a reduction in the mean, minimum, and maximum groundwater levels, except for a smaller rise in the southwest.

6.6. SMDI and ETDI

Fig. 6 shows the spatial distribution of the SMDI and ETDI in the study area; the top row in the figures is the driest week (from the indexing) for the historical period, the RCP4.5 and the 6 degree scenarios. The bottom row on the figures shows the percentage of weeks where the index is below −3 for each grid. Fig. 7 shows the accumulated distribution of the SMDI and ETDI index for the whole catchment. The dashed line shows the driest occurring week, corresponding to the weeks presented on Fig. 6, while the solid lines represent the distribution of the index during all summer weeks for the entire period.

The driest week in the historical period (Fig. 6A) results in scattered locations of dry areas with SMDI between −3 and −4, where 63% of all grids are below

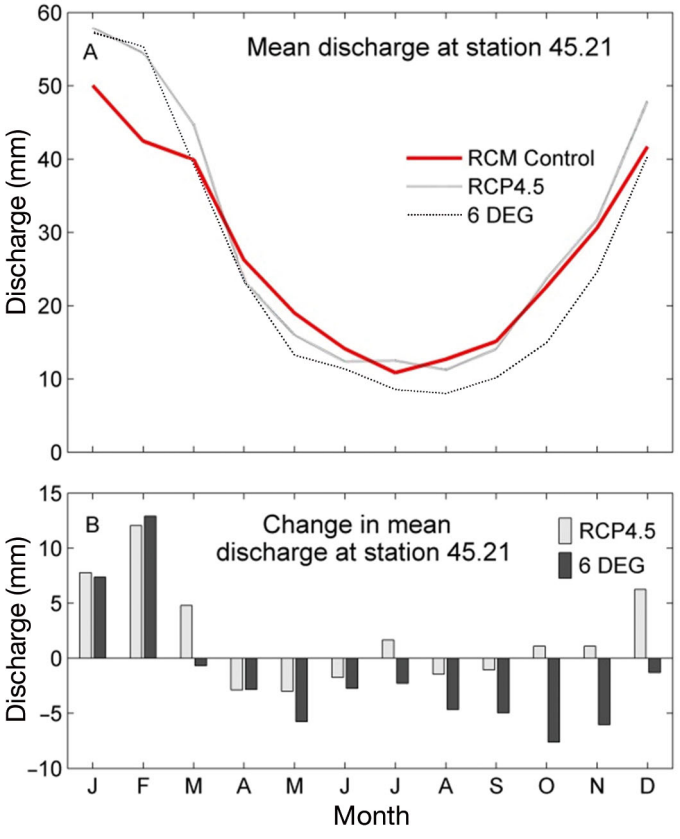

Fig. 4. (A) Mean monthly discharge at the main station (45.21) of the catchment for 2 emission scenarios (RCP4.5 and 6 degree) and the RCM control period, and (B) their respective relative change (in mm) from the RCM historical control period. Note: this is a hydrological model run without CO_2-correction on reference evapotranspiration

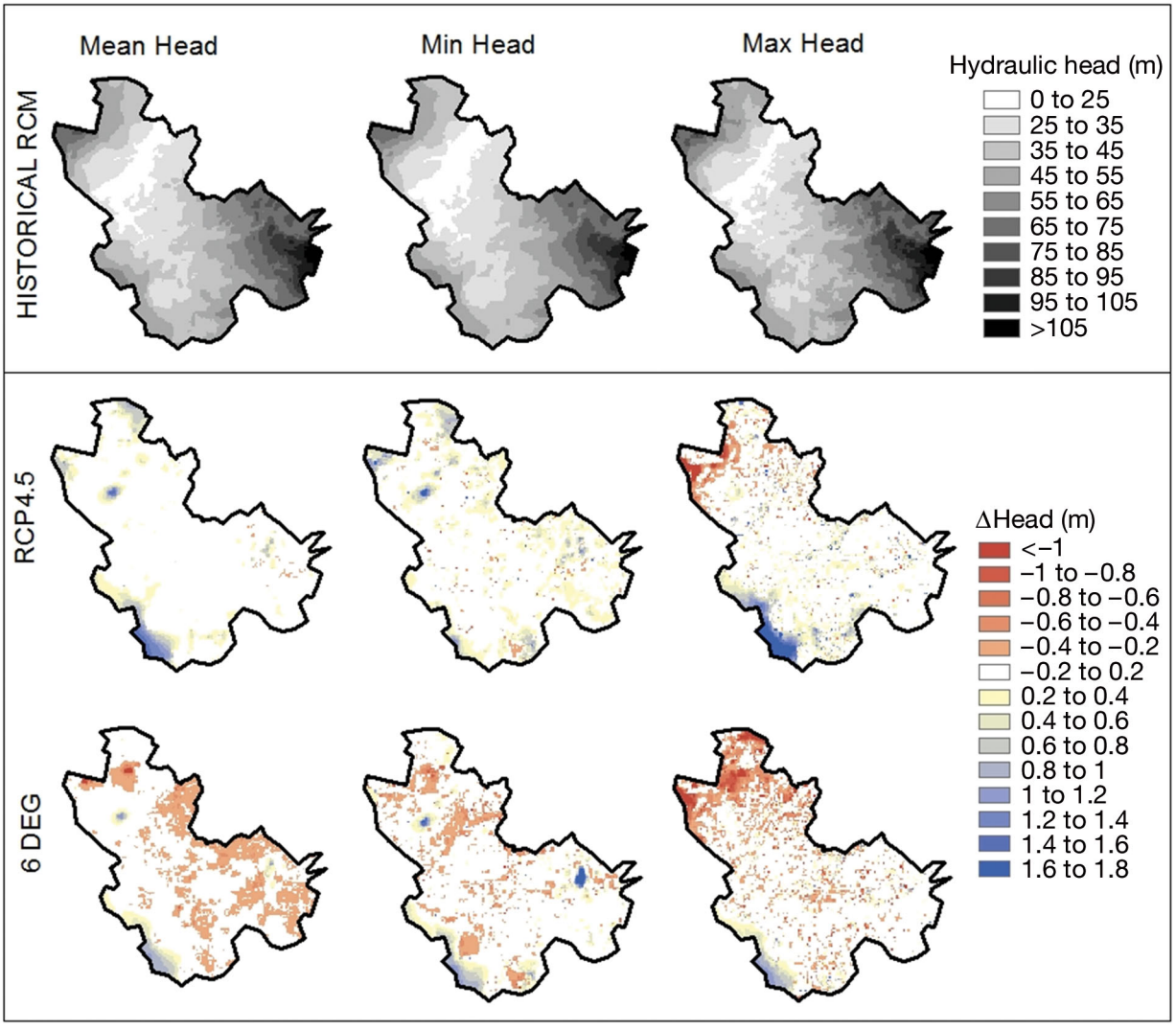

Fig. 5. Top row: mean, minimum and maximum hydraulic head for the historical RCM simulation. Bottom 2 rows: change in mean, min. and max. head from the historical RCM control period to the RCP4.5 and the 6 degree scenario future period (no CO_2-correction). Red: reduction of the head values in the future; Blue: increase in head value. Head values: top layer

−3 (Fig. 7A). For the RCP4.5 the area becomes even drier (92% is below −3), with the driest areas present in the south. Moving on to the 6 degree scenario, a drought is realized in almost the entire catchment, with SMDI values below −4 for most of the area (96% is below −3; 72% is below −4). Looking at the percentage of weeks with dry conditions, a similar signal is found with increasing dryness from RCP4.5 to the 6 degree scenario, where >70% of all grids experience SMDI below −3 more than 10% of the time. This is also apparent on Fig. 7A for the summer weeks index distribution. Here, the graphs for the 2 future periods are both offset to the left indicating increasing dryness. The largest difference between the historical period and the 6 degree scenario is found for the driest index values.

The ETDI shows that the RCP4.5 has a less extreme driest week than the historical period (Fig. 6B), even though over the whole period the RCP4.5 has more grids with dry days. Also the total response from the summer weeks (Fig. 7B) shows a close resemblance to the historical period distribution, with a smaller tendency towards a drying offset for the driest indices. The 6 degree scenario is still the driest with 24% of all grids below −4 in the driest week. This week, however, also shows that even though the driest indices become drier, the less dry (above −4) actually become wetter (Fig. 7B). As with the SMDI, the largest difference in index distribution for the historical and the 6 degree scenario is found in the driest indices. The overall drying signal is not as significant for the ETDI as for the SMDI, which may point out the

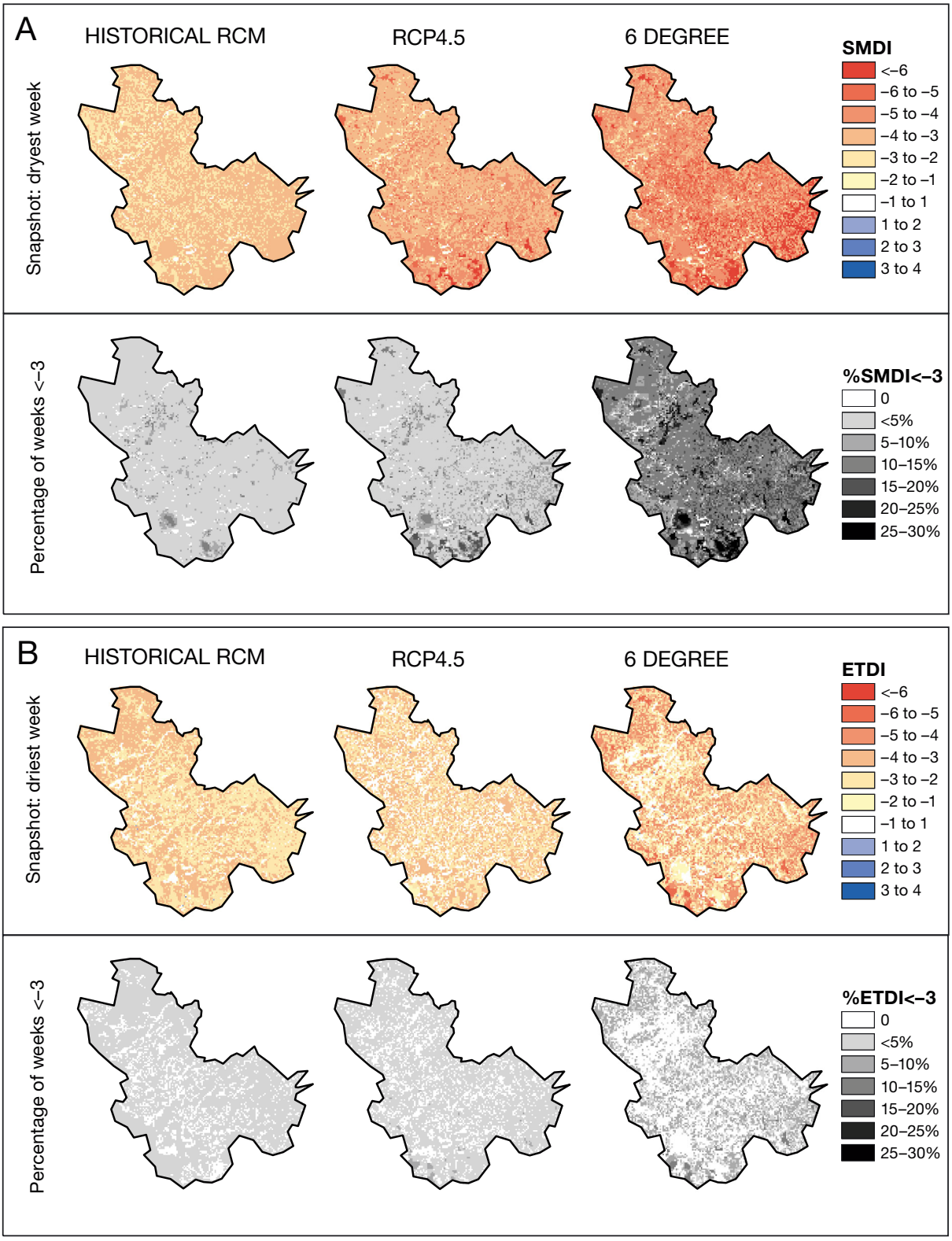

Fig. 6. (A) Soil moisture deficit index (SMDI) and (B) evapotranspiration deficit index (ETDI). Top row: driest week in the simulation period as a snapshot in time for the historical RCM simulation and the 2 future simulations from the RCP4.5 and the 6 degree scenario future period (no CO_2-correction). Bottom row: percentage of weeks during the simulation period where SMDI/EIDI were below –3 for each grid in the catchment

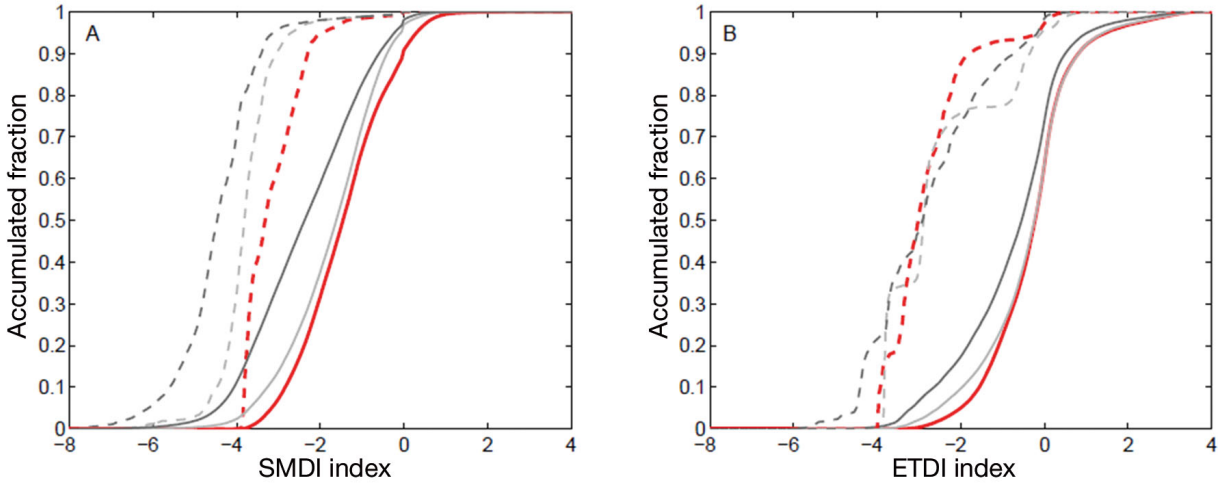

Fig. 7. Accumulated distribution of the (A) SMDI and (B) ETDI in all catchment grids in the control/future period. Red: RCM control; light grey: RCP4.5; dark grey: 6DEG. Distributions are shown both for the driest week (dashed lines) and for all the summer weeks (solid lines)

differences in the 2 indices, as SMDI only covers the top 30 cm of the root zone, while the ETDI represents the overall signal for the soil moisture available for plant transpiration in the entire root zone. On both index maps—more so for ETDI—the location of the river can be recognized (Fig. 6).

7. DISCUSSION

In this study, climate variables from a high-end 6 degree emission scenario were bias-corrected and used in a distributed hydrological model for the Odense sub-catchment in central Denmark. The impact on hydrology and agricultural drought was then evaluated. Furthermore the high-end scenario was compared with a medium emission scenario, the RCP4.5, from the same GCM/RCM model combination, and to some degree with results from A1B scenario runs with multiple GCM/RCM combinations.

7.1. Characteristic of the high-end 6 degree scenario

The 6 degree scenario is characterized by large year round temperature increases of up to 5.7°C, with increasing reference evapotranspiration as a result. Precipitation especially increases in winter and autumn, while summer experiences a decrease in precipitation. For the Odense sub-catchment, this means an annual precipitation change of +7% from the historical to future period (RCM-GCM values), compared to a +6% change in the RCP4.5. The 6 degree emission scenario results in large changes in the hydrology of the catchment. In spite of the precipitation increase, the actual evapotranspiration increase of +17% for the 6 degree scenario causes decreasing stream discharge for most of the year. This is especially critical in the summer period where stream flow is already low, potentially leading to problematic ecological consequences as stream and wetland desiccation. Furthermore, the changes also lead to increasing difference in stream flow between the seasons as January and February have the highest discharge values and will experience further increase in the future.

The risk of drying-out is also evident from the overall lowering of the groundwater table in the catchment. The reason for the increased groundwater level in the southwest of the catchment may be due to greater depth of the groundwater table, implying that even though the groundwater level rises in response to the higher winter precipitation, it is still too deep for root zone water uptake. Conversely, the shallow groundwater table in the majority of the catchment enables the crops to extract water and thereby increase the evapotranspiration, and thus reduce the groundwater level.

7.2. CO_2 effect

The effect of increasing CO_2 is, in this study, described by a relatively simple approach where a factor is multiplied on the reference evapotranspiration to mimic the reduction in transpiration of the plants. However, the effect of CO_2 on plant evapotranspiration is still highly uncertain (see e.g. Zhu et al. 2012)

and affected by several factors. CO_2 acts as a plant fertilizer and an increase in CO_2 could cause an increase in aboveground biomass and hence leaf area index, which will have a positive influence on evapotranspiration that may counteract the effect of stomata closure. This was shown experimentally by Qiao et al. (2010), where elevated CO_2 did not have any significant effect on evapotranspiration. These dynamic feedbacks on plant physiology are not included in this study, which could be a serious limitation. Further, it is not known at which CO_2-concentration range the approach by Krujit et al. (2008) is valid. The high-end emission scenario considered here results in extremely high CO_2-concentrations, and it is uncertain how the crops react to such a forcing. Finally, using coupled climate–carbon cycle models, Peng et al. (2014) demonstrated that the CO_2-physiological effect on transpiration also significantly affects the precipitation response of the models. Hence, it is difficult to isolate the effect of CO_2 on transpiration and not include the feedback mechanisms on cloud and precipitation formation. Because of these deficiencies in the description of the effects of increasing CO_2-concentration, it was decided not to include this effect in the final model simulations. However, this mechanism adds uncertainty to the results and more research should be done to quantify this effect.

7.3. Inter-model variability vs. emission scenario variability

Several studies have shown that the influence of the choice of climate model is more important than the choice of the emission scenario (Hawkins & Sutton 2011, IPCC 2013), as the spread in model results is large. These studies have been based on emission scenarios from the normal range of emission projections. For some variables and seasons, the present study indicates that when high-end scenarios are included in the impact studies, the choice of emission projection can be more important than the climate model choice. This finding should, however, be considered with caution, because we do not have ensemble results for the high-end scenario, but only for the moderate A1B scenario (ENSEMBLES runs).

7.4. Indices and usability

The indices SMDI and ETDI were developed by Narasimhan & Srinivasan (2005), and to our knowledge this is the first time the indices have been used to evaluate future climate change impacts on the root zone water balance. Narasimhan & Srinivasan (2005) found a good correlation between wheat and sorghum crop yield and the index response. While further studies may be needed to document the general applicability of these indices as good indicators of crop yield, the study by Narasimhan & Srinivasan (2005) indicates that the use of indices on soil moisture data and/or evapotranspiration data from a hydrological model can be used as an initial evaluation tool to assess future climate change impact on crop yield, thereby saving substantial time on complex agricultural and hydrological model combinations.

8. CONCLUSION

This study has evaluated the impact of a high-end 6 degree emission scenario on hydrology and soil moisture in a Danish agricultural catchment. The high-end scenario showed larger temperature increases and large changes in reference evapotranspiration and precipitation. The stream discharge impact caused larger seasonal differences from winter to summer, as winter discharge increased while most of the remaining year had decreasing discharge values. Generally the climate change resulted in a lowering of the groundwater head and a substantial increase of dryness in the root zone, represented by an overall lowering of the agricultural indices. Altogether, the most prominent changes in the water balance were found due to drying out of soils rather than precipitation effects.

Acknowledgements. The present study was funded by a grant from the Danish Strategic Research Council for the Centre for Regional Change in the Earth System (CRES – www.cres-centre.dk) under contract no: DSF-EnMi 09-066868. We also acknowledge the help received from Christen Duus Børgesen, Department of Agroecology – Climate and Water at Aarhus University, Denmark in connection with the implementation of vegetation properties in the model.

LITERATURE CITED

Abbott MB, Bathurst JC, Cunge JA, O'Connell PE, Rasmussen J (1986) An introduction to the European hydrological system – Systeme Hydrologique Europeen, 'SHE'. 2. Structure of a physically-based, distributed modelling system. J Hydrol 87:61–77

Allen RG, Pereira LS, Raes D, Smith M (1998) Crop evapotranspiration: guidelines for computing crop water requirements. FAO Irrigation and Drainage Paper 56, FAO, Rome

Arnell NW (1999) Climate change and global water resources. Glob Environ Change 9(Supplement 1):S31–S49

Arnold JG, Srinivasan R, Muttiah RS, Williams JR (1998) Large area hydrologic modelling and assessment. 1. Model development. J Am Water Resour Assoc 34:73–89

Bergström S, Carlsson B, Gardelin M, Lindström G, Pettersson A, Rummukainen M (2001) Climate change impacts on runoff in Sweden: assessments by global climate models, dynamical downscaling and hydrological modelling. Clim Res 16:101–112

Børgesen CD, Jensen PN, Blicher-Mathiesen G, Schelde K and others (2013) Udviklingen i kvælstofudvaskning of næringsstofoverskud fra dansk landbrug for perioden 2007–2011. Evaluering af implementerede virkemidler til reduktion af kvælstofudvaskning samt en fremskrivning af planlagte virkemidlers effekt frem til 2015. In: Børgesen CD, Jensen PN, Blicher-Mathiesen G, Schelde K (eds) DCA Rapport, Nr. 031, DCA, Tjele

Christensen OB, Drews M, Christensen JH, Dethloff K, Ketelsen K, Hebestadt I, Rinke A (2007) The HIRHAM Regional Climate Model Version 5 (β). DMI Tech Rep 06-17, DMI, Copenhagen

Christensen OB, Yang S, Boberg F, Fox Maule C and others (2015) Scalability of regional climate change in Europe for high-end scenarios. Clim Res 64:25–38

Clarke L, Edmonds J, Jacoby H, Pitcher H, Reilly J, Richels R (2007) Scenarios of greenhouse gas emissions and atmospheric concentrations. Sub-report 21A of Synthesis and Assessment Product 2.1 by the US Climate Change Science Program and the Subcommittee on Global Change Research, Department of Energy, Washington, DC

Collins M, Knutti R, Arblaster J, Dufresne JL and others (2013) Long-term climate change: projections, commitments and irreversibility. In: Stocker TF, Qin D, Plattner G-K, Tignor M and others (eds) Climate Change 2013: the physical science basis. Contribution of Working Group I to the Fifth Assessment Report of the Intergovernmental Panel on Climate Change. Cambridge University Press, Cambridge

Conley MM, Kimball BA, Brooks TJ, Pinter PJ and others (2001) CO_2 enrichment increases water-use efficiency in sorghum. New Phytol 151:407–412

Déqué M, Rowell D, Lüthi D, Giorgi F and others (2007) An intercomparison of regional climate simulations for Europe: assessing uncertainties in model projections. Clim Change 81:53–70

DHI (2009a) AutoCal: autocalibration tool. In: DHI (ed) Mike Zero 2009. DHI, Water & Environment, Hørsholm, p 1–42

DHI (2009b) Reference guide. In: DHI (ed) MIKE SHE User Manual, Book 2. DHI, Water & Environment, Hørsholm, p 132–168 and 345–367

Environment Centre Odense (2007) Odense pilot river basin. Pilot project for river basin management planning. In: Madsen HB, Pedersen SE, Kristensen ND, Jørgensen OT (eds) Water Framework Directive Article 13. Danish Ministry of the Environment, Environment Centre Odense, Odense

GEUS (Geological Survey of Denmark and Greenland) (2014) National well database JUPITER, available at www.geus.dk/DK/data-maps/jupiter/Sider/default.aspx (accessed February 2014)

Greve MH, Greve MB, Bøcher PK, Balstrøm T, Madsen HB, Krogh L (2007) Generating a Danish raster-based topsoil property map combining choropleth maps and point information. Geogr Tidsskr 107(2):1–12

Hansen S, Jensen HE, Nielsen NE, Svendsen H (1990) DAISY: soil–plant–atmosphere system model. NPO Res Rep A10, The National Agency for Environmental Protection, Copenhagen

Hawkins E, Sutton R (2011) The potential to narrow uncertainty in projections of regional precipitation change. Clim Dyn 37:407–418

Hazeleger W, Wang X, Severijns C, Ştefănescu S and others (2012) EC-Earth V2.2: description and validation of a new seamless earth system prediction model. Clim Dyn 39:2611–2629

Henriksen HJ, Troldborg L, Nyegaard P, Sonnenborg TO, Refsgaard JC, Madsen B (2003) Methodology for construction, calibration and validation of a national hydrological model for Denmark. J Hydrol 280:52–71

Hewitt CD, Griggs DJ (2004) Ensembles-based predictions of climate changes and their impacts. EOS Trans AGU 85:566–566

Hill MC (1998) Methods and guidelines for effective model calibration. Water Resour Invest Rep 98-4005. USGS, Denver, CO

Højberg AL, Troldborg L, Stisen S, Christensen BSB, Henriksen HJ (2013) Stakeholder driven update and improvement of a national water resources model. Environ Model Software 40:202–213

IPCC (Intergovernmental Panel on Climate Change) (2001) Climate change 2001: the scientific basis. Contribution of Working Group I to the Third Assessment Report of the Intergovernmental Panel on Climate Change. In: Houghton JT, Ding Y, Griggs DJ, Noguer M and others (eds) IPCC Third Assessment Report. Cambridge University Press, Cambridge

IPCC (2013) Climate Change 2013: the physical science basis. Contribution of Working Group I to the Fifth Assessment Report of the Intergovernmental Panel on Climate Change. In: Stocker TF, Qin D, Plattner G-K, Tignor M and others (eds) IPCC Fifth Assessment Report (AR5). Cambridge University Press, Cambridge

Karlsson IB, Refsgaard JC, Sonnenborg TO, Jensen KH (2014) Significance of hydrological model choice when doing climate change impact assessment. EGU General Assembly, 27 April– 2 May 2014, Vienna

Kimball BA, Mauney JR, Nakayama FS, Idso SB (1993) Effects of increasing atmospheric CO_2 on vegetation. Vegetatio 104-105:65–75

Kimball BA, LaMorte RL, Pinter PJ Jr, Wall GW and others (1999) Free-air CO_2 enrichment and soil nitrogen effects on energy balance and evapotranspiration of wheat. Water Resour Res 35:1179–1190

Krujit B, Witte JPM, Jacobs C, Kroon T (2008) Effects of rising atmospheric CO_2 on evapotranspiration and soil moisture: a practical approach for the Netherlands. J Hydrol 349:257–267

Makkink GF (1957) Testing the Penman formula by means of lysimeters. J Inst Water Eng Sci 11:277–288

Meinshausen M, Smith SJ, Calvin K, Daniel JS and others (2011) The RCP greenhouse gas concentrations and their extensions from 1765 to 2300. Clim Change 109: 213–241

Nakicenovic N, Alcamo J, Davis G, de Vries B and others (2000) Emission scenarios. In: Nakicenovic N, Swart R (eds) Emission scenarios. Cambridge University Press, Cambridge

Narasimhan B, Srinivasan R (2005) Development and evaluation of soil moisture deficit index (SMDI) and evapotranspiration deficit index (ETDI) for agricultural drought monitoring. Agric For Meteorol 133:69–88

Nyegaard P, Troldborg L, Højberg AL (2010) DK-model 2009: Geologisk og hydrostratigrafisk opdatering 2005–2009. GEUS Rep 2010/80, Copenhagen

Peng J, Dan L, Dong W (2014) Are there interactive effects of physiological and radiative forcing produced by increased CO2 concentration on changes of land hydrological cycle? Global Planet Change 112:64–78

Piani C, Haerter JO, Coppola E (2010) Statistical bias correction for daily precipitation in regional climate models over Europe. Theor Appl Climatol 99:187–192

Qiao Y, Zhang H, Dong B, Shi C, Li Y, Zai H, Lui M (2010) Effects of elevated CO2 concentration on growth and water use efficiency of winter wheat under two soil water regimes. Agric Water Manag 97:1742–1748

Rasmussen J, Sonnenborg TO, Stisen S, Seaby LP, Christensen BSB, Hinsby K (2012) Climate change effects on irrigation demands and minimum stream discharge: impact of bias-correction method. Hydrol Earth Syst Sci 16:4675–4691

Samarakoon AB, Gifford RM (1995) Soil water content under plants at high CO_2 concentration and interactions with the direct CO_2 effects: a species comparison. J Biogeogr 22:193–202

Scharling M (1999) Klimagrid Danmark: nedbør 10 × 10 km. Metodebeskrivelse. DMI Tech Rep 99-15. DMI, Copenhagen

Seaby LP, Refsgaard JC, Sonnenborg TO, Stisen S, Christensen JH, Jensen KH (2013) Assessment of robustness and significance of climate change signals for an ensemble of distribution-based scaled climate projections. J Hydrol 486:479–493

Seaby LP, Refsgaard JC, Sonnenborg TO, Højberg AL (2015) Spatial uncertainty in bias corrected climate change projections and hydrological impacts. Hydrol Processes (in press) doi:10.1002/hyp.10501

Smith SJ, Wigley T (2006) Multi-gas forcing stabilization with MiniCAM. Energy J Spec Issue 3:373–392

Stisen S, Højberg AL, Troldborg L, Refsgaard JC, Christensen BSB, Olsen M, Henriksen HJ (2012) On the importance of appropriate precipitation gauge catch correction for hydrological modelling at mid to high latitudes. Hydrol Earth Syst Sci 16:4157–4176

Thomson AM, Calvin KV, Smith SJ, Kyle GP and others (2011) RCP4.5: a pathway for stabilization of radiative forcing by 2100. Clim Change 109:77–94

Troldborg L, Højberg AL, Nyegaard P, Stisen S, Christensen BSB, Ondracek M (2010) DK-model2009: Modelopstilling og kalibrering for Fyn. GEUS Rep 2010/76, Copenhagen

van Roosmalen L, Christensen BSB, Sonnenborg TO (2007) Regional differences in climate change impacts on groundwater and stream discharge in Denmark. Vadose Zone J 6:554–571

van Vuuren D, Edmonds J, Kainuma M, Riahi K and others (2011) The representative concentration pathways: an overview. Clim Change 109:5–31

Wise M, Calvin K, Thomson A, Clarke L and others (2009) Implications of limiting CO_2 concentrations for land use and energy. Science 324:1183–1186

Zhu Q, Jiang H, Peng C, Liu J and others (2012) Effects of future climate change, CO_2 enrichment, and vegetation structure variation on hydrological processes in China. Global Planet Change 80–81:123–135

Submitted: May 15, 2014; Accepted: September 24, 2014

Proofs received from author(s): April 24, 2015